Adaptive Signal Processing Method Using a Single-Element Dual-Polarized Antenna for GNSS Interference Mitigation

Kwansik Park, *Yonsei University, South Korea*
Dongkoog Lee, *Agency for Defense Development, South Korea*
Jiwon Seo, *Yonsei University, South Korea*

BIOGRAPHIES

Kwansik Park is a Ph.D. student at the School of Integrated Technology, Yonsei University, Korea. He received his B.S. degree in electrical and electronic engineering from Yonsei University in 2012. His current research mainly focuses on GPS anti-interference technologies.

Dongkoog Lee received his M.S. degree in electronic engineering from Kyungpook University, Daegu, Korea, in 2000. He is a senior researcher in the Radar Department, Agency for Defense Development (ADD), Korea. His research interests are focused on phased-array antennas for multifunction radar systems.

Jiwon Seo received his B.S. degree in mechanical engineering (division of aerospace engineering) from Korea Advanced Institute of Science and Technology, Daejeon, Korea. Further, he received M.S. degrees in aeronautics/astronautics and electrical engineering, and a Ph.D. in aeronautics/astronautics from Stanford University, Stanford, CA, USA. He is currently an assistant professor with the School of Integrated Technology, Yonsei University, Korea. Prof. Seo is also a member of the International Advisory Council of the Resilient Navigation and Timing Foundation, Alexandria, VA, USA, and a member of several advisory committees of the Ministry of Oceans and Fisheries and the Ministry of Land, Infrastructure and Transport, Korea.

ABSTRACT

Due to their weak received power, Global Navigation Satellite Systems (GNSS) signals can be easily disrupted by radio frequency interference. Various GNSS signal processing techniques using single-antenna-based methods and antenna-array-based methods have been addressed in the literature to mitigate the interference, as well as to enhance the desired GNSS signals. However, single-antenna techniques do not successfully suppress wideband interference in general, and the computational complexity, as well as the large size and high cost of the antenna array, still remain as barriers to numerous applications. To obtain interference mitigation performance while reducing hardware complexity, the polarization diversity provided by single-element dual-polarized antennas has also been studied. However, to the best of the authors' knowledge, the previous works can mitigate only one source of interference at a time, or only interference with a certain polarization (e.g., linearly-polarized interference only). This paper proposes an adaptive signal processing method for a single-element dual-polarized antenna. Similar to spatial-temporal adaptive processing algorithms for antenna arrays, our method can mitigate one wideband interference signal in the spatial domain by exploiting polarization diversity while mitigating the narrowband interference in the frequency domain using finite impulse response (FIR) filters. We consider right-hand circularly polarized (RHCP), left-hand circularly polarized (LHCP), and linearly polarized (LP) interference signals, and it is shown that our method has the capability to simultaneously suppress one wideband and multiple narrowband interferences with any of the three polarizations (i.e., RHCP, LHCP, and LP). For a demonstration of our method, simulation is performed with one wideband and multiple narrowband interference signals, which have different polarizations, in the test scenario. Using the weight vector obtained by the proposed algorithm, the angle–frequency response, frequency responses with respect to the three polarizations, and signal-to-interference-plus-noise-ratio plots are presented.

INTRODUCTION

The vulnerability of Global Navigation Satellite Systems (GNSS) receivers to radio frequency interference (RFI) has been emphasized in the field of GNSS due to the weak power of received GNSS signals [1–6], which is typically lower than the thermal noise floor [7]. Ionospheric anomalies can also impact GNSS signals [8–13]. As countermeasures, there have been intensive researches regarding signal processing techniques to mitigate GNSS interference, and these signal processing methods can be divided into antenna-array-based methods [14–17] and single-antenna-based methods [18–21].

Antenna-array-based techniques [14–17] utilize antenna arrays, which consist of spatially distributed multiple antenna elements. Spatial processing using the antenna array can generate spatial nulls in the directions of multiple wideband interference signals because the array geometry can provide spatial degrees of freedom (DOFs). The performance of the antenna arrays can be improved further by spatial-temporal adaptive processing (STAP) [22, 23], which is typically implemented by attaching finite impulse response (FIR) filters to the antenna elements, so that multiple narrowband interference signals can also be suppressed in the frequency domain. However, even though the antenna-array-based methods have shown good performance, the inevitable large array size, high cost, and computational complexity still remain as challenges.

On the other hand, the single-antenna-based techniques [18–21] utilize various digital filtering techniques to mitigate multiple narrowband interference signals. However, although the conventional single-antenna-based methods can be implemented more simply when compared to the antenna arrays, wideband interference signals cannot be suppressed by the single-antenna method due to a lack of spatial DOFs. As an attempt to resolve this insufficient capability of wideband interference mitigation, polarization diversity has drawn attention. As the spatial DOFs can be provided from the spatial diversity of the antenna array, the polarization diversity of dual-polarized antennas may also provide DOFs. As a dual-polarized antenna, which can receive two orthogonally polarized signals simultaneously, possesses the polarization diversity, it has been studied for interference mitigation in literature. However, to the best of the authors' knowledge, the previous works regarding the dual-polarized antenna [24–26] can mitigate only one interference source at a time, or interference signals with a certain polarization.

In this paper, we present an adaptive signal processing method using a single-element dual-polarized antenna. In our approach, the polarization of the interference signals can be any combination of right-hand circular polarization (RHCP), left-hand circular polarization (LHCP), and linear polarization (LP), and the proposed method can successively mitigate multiple interference sources simultaneously, even when they have different polarizations. Since our method was motivated by conventional STAP algorithms for GNSS antenna arrays, our method has the capability to mitigate one wideband and multiple narrowband interference signals simultaneously with no prior knowledge of the interference polarizations and directions. To calculate the weight vector for interference suppression, we adopted the least mean square (LMS) algorithm [27], which can mitigate the impact of interference by minimizing the error between the output signal from our signal processing structure and the locally generated GNSS signal. For a performance demonstration of our method, we perform a simulation for an interference scenario in which one wideband and three narrowband interference signals of different polarizations are injected. From the simulation results, angle–frequency response, frequency response, and signal to interference-plus-noise power ratio (SINR) plots are provided, and these results validate the interference mitigation capability of the proposed single-element dual-polarized antenna solution.

RECEIVED SIGNAL MODEL

We consider three types of incoming signals, namely, RHCP, LHCP, and LP signals. The polarization states of these three signals traveling along the $-\hat{\mathbf{r}}$ direction in the spherical coordinates of Figure 1 can be mathematically described using the complex vector representation of their electric fields, as follows [28]:

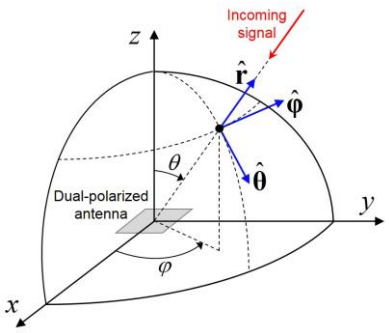

Figure 1: Coordinate system for the single-element dual-polarized antenna. $\hat{\boldsymbol{\theta}}$, $\hat{\boldsymbol{\varphi}}$, and $\hat{\mathbf{r}}$ are the unit vectors of the spherical coordinates

$$\begin{aligned}
\mathbf{E}_{\mathrm{R}}(\theta,\varphi) &= \frac{E_{\mathrm{R}0}}{\sqrt{2}}\left(\hat{\boldsymbol{\theta}} + j\hat{\boldsymbol{\varphi}}\right) \equiv E_{\mathrm{R}0}\hat{\mathbf{E}}_{\mathrm{R}}(\theta,\varphi) \\
\mathbf{E}_{\mathrm{L}}(\theta,\varphi) &= \frac{E_{\mathrm{L}0}}{\sqrt{2}}\left(\hat{\boldsymbol{\theta}} - j\hat{\boldsymbol{\varphi}}\right) \equiv E_{\mathrm{L}0}\hat{\mathbf{E}}_{\mathrm{L}}(\theta,\varphi) \\
\mathbf{E}_{\mathrm{Lin}}(\theta,\varphi,\alpha) &= E_{\mathrm{Lin}0}\left(\cos\alpha\,\hat{\boldsymbol{\theta}} + \sin\alpha\,\hat{\boldsymbol{\varphi}}\right) \equiv E_{\mathrm{Lin}0}\hat{\mathbf{E}}_{\mathrm{Lin}}(\theta,\varphi,\alpha)
\end{aligned}, \tag{1}$$

where $\hat{\boldsymbol{\theta}}$, $\hat{\boldsymbol{\varphi}}$, and $\hat{\mathbf{r}}$ are the unit vectors of the spherical coordinates; $E_{\mathrm{R}0}$, $E_{\mathrm{L}0}$, and $E_{\mathrm{lin}0}$ are the amplitudes of the RHCP, LHCP, and LP signal, respectively; and α is the tile angle, as shown in Figure 2.

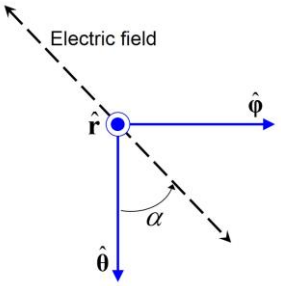

Figure 2: Two-dimensional view of an LP signal propagating along the $-\hat{\mathbf{r}}$ direction in Figure 1. The dashed arrow indicates the oscillation direction of the electric field, and α is the tilt angle of the electric field oscillation from the direction of the unit vector $\hat{\boldsymbol{\theta}}$ toward the direction of the unit vector $\hat{\boldsymbol{\varphi}}$.

In addition, a single-element dual-polarized antenna, which is located at the origin and consists of RHCP and LHCP antenna components, is considered in Figure 1. The radiation pattern and polarization of an antenna can be characterized using a complex vector, which is called the complex radiation field. A circularly polarized antenna can be considered a combination of two linearly polarized antennas out of phase by 90° (RHCP) or -90° (LHCP) [29], and we assume that the RHCP and LHCP antenna components are implemented by two short dipoles, which are aligned with the *x*- and *y*-axis. The complex radiation fields of these short dipoles are given as follows [30].

$$\begin{aligned}
\mathbf{G}_{\mathrm{x}}(\theta,\varphi) &= G_0\left(\cos\theta\cos\varphi\hat{\boldsymbol{\theta}} - \sin\varphi\hat{\boldsymbol{\varphi}}\right) \\
\mathbf{G}_{\mathrm{y}}(\theta,\varphi) &= G_0\left(\cos\theta\sin\varphi\hat{\boldsymbol{\theta}} + \cos\varphi\hat{\boldsymbol{\varphi}}\right)
\end{aligned}, \tag{2}$$

where G_0 is the maximum magnitude of $\mathbf{G}_{\mathrm{x}}(\theta,\varphi)$ and $\mathbf{G}_{\mathrm{y}}(\theta,\varphi)$. From (1), the complex radiation fields of the RHCP and LHCP antenna components can be obtained as follows:

$$\begin{aligned}
\mathbf{G}_{\mathrm{R}}(\theta,\varphi) &= \frac{1}{\sqrt{2}}\left\{\mathbf{G}_{\mathrm{x}}(\theta,\varphi) + j\mathbf{G}_{\mathrm{y}}(\theta,\varphi)\right\} \\
&= \frac{G_0}{\sqrt{2}}\left\{\left(\cos\theta\cos\varphi + j\cos\theta\sin\varphi\right)\hat{\boldsymbol{\theta}} + \left(-\sin\varphi + j\cos\varphi\right)\hat{\boldsymbol{\varphi}}\right\} \\
&\equiv G_0\hat{\mathbf{G}}_{\mathrm{R}}(\theta,\varphi) \\
\mathbf{G}_{\mathrm{L}}(\theta,\varphi) &= \frac{1}{\sqrt{2}}\left\{\mathbf{G}_{\mathrm{x}}(\theta,\varphi) - j\mathbf{G}_{\mathrm{y}}(\theta,\varphi)\right\} \\
&= \frac{G_0}{\sqrt{2}}\left\{\left(\cos\theta\cos\varphi - j\cos\theta\sin\varphi\right)\hat{\boldsymbol{\theta}} + \left(-\sin\varphi - j\cos\varphi\right)\hat{\boldsymbol{\varphi}}\right\} \\
&\equiv G_0\hat{\mathbf{G}}_{\mathrm{L}}(\theta,\varphi)
\end{aligned}. \tag{3}$$

When a signal is incident on a receiving antenna, a voltage induced over the antenna due to the signal is proportional to the inner product between the complex radiation fields of the antenna and the electric field vector of the incoming signal [31]. Therefore, the two voltages induced over the RHCP and LHCP components of the dual-polarized antenna can be expressed as follows:

$$\begin{aligned} V_{\mathrm{R}} &= K\,\mathbf{G}_{\mathrm{R}}(\theta,\varphi)\cdot\mathbf{E}^{*} \\ &= KG_0E_0\left\{\hat{\mathbf{G}}_{\mathrm{R}}(\theta,\varphi)\cdot\hat{\mathbf{E}}^{*}\right\}, \\ V_{\mathrm{L}} &= K\,\mathbf{G}_{\mathrm{L}}(\theta,\varphi)\cdot\mathbf{E}^{*} \\ &= KG_0E_0\left\{\hat{\mathbf{G}}_{\mathrm{L}}(\theta,\varphi)\cdot\hat{\mathbf{E}}^{*}\right\} \end{aligned} \tag{4}$$

where E_0 and $\hat{\mathbf{E}}$ can be one of $\{E_{\mathrm{R}0}, E_{\mathrm{L}0}, E_{\mathrm{Lin}0}\}$, $\{\hat{\mathbf{E}}_{\mathrm{R}}(\theta,\varphi), \hat{\mathbf{E}}_{\mathrm{L}}(\theta,\varphi), \hat{\mathbf{E}}_{\mathrm{Lin}}(\theta,\varphi,\alpha)\}$, respectively. The inner products in (4) characterize variations of the incoming signal due to the effects of the radiation pattern and polarization when the signal is received by the two antenna components of the dual-polarized antenna.

ADAPTIVE SIGNAL PROCESSING

Based on the received signal model shown in the previous section, an adaptive signal processing method, which is implemented as shown in Figure 3, is proposed. The FIR filters are attached to the two components of the dual-polarized antenna.

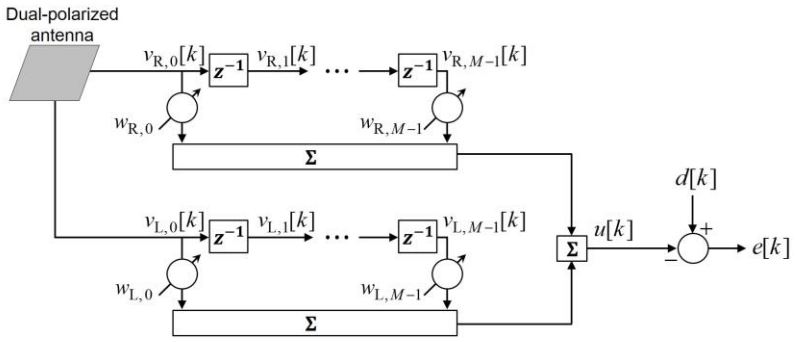

Figure 3: Block diagram of the proposed adaptive signal processing structure for the single-element dual-polarized antenna.

The output signal is equal to the summation of the weighted signals from all the time taps, as follows:

$$\begin{aligned} u[k] &= \sum_{m=0}^{M-1}\left(w_{\mathrm{R},m}^{*}v_{\mathrm{R},m}[k] + w_{\mathrm{L},m}^{*}v_{\mathrm{L},m}[k]\right), \\ &= \mathbf{w}^{H}\mathbf{v}[k] \end{aligned} \tag{5}$$

where $\mathbf{w}$ and $\mathbf{v}[k]$ are the weight vector and signal vector,

$$\begin{aligned} \mathbf{w} &= \begin{bmatrix} w_{\mathrm{R},0} & w_{\mathrm{L},0} & \cdots & w_{\mathrm{R},M-1} & w_{\mathrm{L},M-1} \end{bmatrix}^{T} \\ \mathbf{v}[k] &= \begin{bmatrix} v_{\mathrm{R},0}[k] & v_{\mathrm{L},0}[k] & \cdots & v_{\mathrm{R},M-1}[k] & v_{\mathrm{L},M-1}[k] \end{bmatrix}^{T} \\ v_{\mathrm{R},m}[k] &= v_{\mathrm{R},0}[k-m] \\ v_{\mathrm{L},m}[k] &= v_{\mathrm{L},0}[k-m] \end{aligned} . \tag{6}$$

If there are N_{GPS} GPS signals and N_{I} interference signals, $v_{\mathrm{R},m}[k]$ and $v_{\mathrm{L},m}[k]$ can be represented as follows:

$$v_{\mathrm{R},m}[k] = KG_0\left[\sum_{n_{\mathrm{GPS}}=1}^{N_{\mathrm{GPS}}}\left\{\mathbf{G}_{\mathrm{R}}\left(\theta_{n_{\mathrm{GPS}}},\varphi_{n_{\mathrm{GPS}}}\right)\cdot\hat{\mathbf{E}}_{\mathrm{R}}\left(\theta_{n_{\mathrm{GPS}}},\varphi_{n_{\mathrm{GPS}}}\right)s_{\mathrm{GPS},\,n_{\mathrm{GPS}}}[k]\right\}+\sum_{n_{\mathrm{I}}=1}^{N_{\mathrm{I}}}\left\{\mathbf{G}_{\mathrm{R}}\left(\theta_{n_{\mathrm{I}}},\varphi_{n_{\mathrm{I}}}\right)\cdot\hat{\mathbf{E}}_{\mathrm{I},\,n_{\mathrm{I}}}\;s_{\mathrm{I},\,n_{\mathrm{I}}}[k]\right\}\right]+\eta_{\mathrm{R},m}[k]$$
$$v_{\mathrm{L},m}[k] = KG_0\left[\sum_{n_{\mathrm{GPS}}=1}^{N_{\mathrm{GPS}}}\left\{\mathbf{G}_{\mathrm{L}}\left(\theta_{n_{\mathrm{GPS}}},\varphi_{n_{\mathrm{GPS}}}\right)\cdot\hat{\mathbf{E}}_{\mathrm{R}}\left(\theta_{n_{\mathrm{GPS}}},\varphi_{n_{\mathrm{GPS}}}\right)s_{\mathrm{GPS},\,n_{\mathrm{GPS}}}[k]\right\}+\sum_{n_{\mathrm{I}}=1}^{N_{\mathrm{I}}}\left\{\mathbf{G}_{\mathrm{L}}\left(\theta_{n_{\mathrm{I}}},\varphi_{n_{\mathrm{I}}}\right)\cdot\hat{\mathbf{E}}_{\mathrm{L},\,n_{\mathrm{I}}}\;s_{\mathrm{I},\,n_{\mathrm{I}}}[k]\right\}\right]+\eta_{\mathrm{L},m}[k]$$
(7)

where $s_{\mathrm{GPS},n_{\mathrm{GPS}}}[k]$ and $s_{\mathrm{I},\,n_{\mathrm{I}}}[k]$ are the n_{GPS}th GPS signal and the n_{I}th interference signal; $(\theta_{n_{\mathrm{GPS}}},\varphi_{n_{\mathrm{GPS}}})$ and $(\theta_{n_{\mathrm{I}}},\varphi_{n_{\mathrm{I}}})$ are the incident angles of $s_{\mathrm{GPS},n_{\mathrm{GPS}}}[k]$ and $s_{\mathrm{I},\,n_{\mathrm{I}}}[k]$; $\hat{\mathbf{E}}_{\mathrm{I},\,n_{\mathrm{I}}}$ is the complex vector representation of the normalized electric field vector corresponding to the n_{I}th interference signal and one of $\{\hat{\mathbf{E}}_{\mathrm{R}}(\theta,\varphi),\hat{\mathbf{E}}_{\mathrm{L}}(\theta,\varphi),\hat{\mathbf{E}}_{\mathrm{Lin}}(\theta,\varphi,\alpha)\}$ according to the interference polarization; and $\eta_{\mathrm{R},m}[k]$ and $\eta_{\mathrm{L},m}[k]$ are the noise components.

For the weight vector calculation, we adopted the least mean square (LMS) algorithm, which minimizes the error $e[k]$ between the output signal $u[k]$ and the locally generated reference signal $d[k]$, as follows [27]:

$$\text{minimize}\,E\left\{\left|e[k]\right|^2\right\} = E\left\{\left|d[k]-u[k]\right|^2\right\}. \tag{8}$$

The optimal weight vector which satisfies (8) is given as follows [27]:

$$\mathbf{w}_{\mathrm{opt}} = \mathbf{R}^{-1}\mathbf{p}, \tag{9}$$

where $\mathbf{R}$ and $\mathbf{p}$ are [27]:

$$\begin{aligned}\mathbf{R} &= E\left\{\mathbf{v}[k]\mathbf{v}^H[k]\right\}\\ \mathbf{p} &= E\left\{\mathbf{v}[k]d^*[k]\right\}\end{aligned}. \tag{10}$$

ANTENNA GAIN PATTERNS

Once the weight vector is computed, the antenna gain patterns generated by our signal processing method can be obtained. Due to the polarization diversity, the gain patterns have a dependency on signal polarization, and we derive the gain patterns corresponding to the three types of signal polarization considered in this study, i.e., RHCP, LHCP, and LP.

Let us first derive the gain pattern with respect to RHCP signals. If there is an RHCP signal impinging on the dual-polarized antenna in the absence of any other signals, the signal vector $\mathbf{v}[k]$ only consists of the received RHCP signal, and the output signal can be rewritten as follows:

$$\begin{aligned}u[k] &= \mathbf{w}^H\mathbf{v}[k]\\ &= \sum_{m=0}^{M-1}\left(w_{\mathrm{R},m}^*v_{\mathrm{R},m}[k]+w_{\mathrm{L},m}^*v_{\mathrm{L},m}[k]\right)\\ &= \sum_{m=0}^{M-1}KG_0\left\{w_{\mathrm{R},m}^*\hat{\mathbf{G}}_{\mathrm{R}}\left(\theta,\varphi\right)\cdot\hat{\mathbf{E}}_{\mathrm{R}}\left(\theta,\varphi\right)s_{\mathrm{R}}[k-m]+w_{\mathrm{L},m}^*\hat{\mathbf{G}}_{\mathrm{L}}\left(\theta,\varphi\right)\cdot\hat{\mathbf{E}}_{\mathrm{R}}\left(\theta,\varphi\right)s_{\mathrm{R}}[k-m]\right\}\\ &= KG_0\sum_{m=0}^{M-1}\left\{w_{\mathrm{R},m}^*\hat{\mathbf{G}}_{\mathrm{R}}\left(\theta,\varphi\right)\cdot\hat{\mathbf{E}}_{\mathrm{R}}\left(\theta,\varphi\right)+w_{\mathrm{L},m}^*\hat{\mathbf{G}}_{\mathrm{L}}\left(\theta,\varphi\right)\cdot\hat{\mathbf{E}}_{\mathrm{R}}\left(\theta,\varphi\right)\right\}s_{\mathrm{R}}[k-m]\end{aligned}, \tag{11}$$

where $s_{\mathrm{R}}[k]$ is the down-converted and sampled version of the incoming RHCP signal.

Then, the Fourier transform, which is applied to the both sides of (11), yields:

$$U(f) = KG_0\sum_{m=0}^{M-1}\left[\left\{w_{\mathrm{R},m}^*\hat{\mathbf{G}}_{\mathrm{R}}\left(\theta,\varphi\right)\cdot\hat{\mathbf{E}}_{\mathrm{R}}\left(\theta,\varphi\right)+w_{\mathrm{L},m}^*\hat{\mathbf{G}}_{\mathrm{L}}\left(\theta,\varphi\right)\cdot\hat{\mathbf{E}}_{\mathrm{R}}\left(\theta,\varphi\right)\right\}\exp\left(-j\frac{2\pi}{f_{\mathrm{s}}}mf\right)S_{\mathrm{R}}(f)\right], \tag{12}$$

where $U(f)$ and $S_{\mathrm{R}}(f)$ are the Fourier transforms of $u[k]$ and $s_{\mathrm{R}}[k]$ and f_{s} is the sampling frequency. From (12), the ratio of $U(f)$ to $S_R(f)$ is given as follows:

$$\begin{aligned}\frac{U(f)}{S_{\mathrm{R}}(f)} &= KG_0 \sum_{m=0}^{M-1}\left[\left\{ w_{\mathrm{R},m}^{*}\hat{\mathbf{G}}_{\mathrm{R}}(\theta,\varphi)\cdot\hat{\mathbf{E}}_{\mathrm{R}}(\theta,\varphi) + w_{\mathrm{L},m}^{*}\hat{\mathbf{G}}_{\mathrm{L}}(\theta,\varphi)\cdot\hat{\mathbf{E}}_{\mathrm{R}}(\theta,\varphi)\right\}\exp\left(-j\frac{2\pi}{f_{\mathrm{s}}}mf\right)\right] \\ &= KG_0 \sum_{m=0}^{M-1}\left[\left\{ w_{\mathrm{R},m}^{*}\frac{1+\cos\theta}{2}\exp(j\varphi) - w_{\mathrm{L},m}^{*}\frac{1-\cos\theta}{2}\exp(-j\varphi)\right\}\exp\left(-j\frac{2\pi}{f_{\mathrm{s}}}mf\right)\right] \\ &\equiv KG_0\, g_{\mathrm{R}}(\theta,\varphi,f)\end{aligned}, \tag{13}$$

where

$$g_{\mathrm{R}}(\theta,\varphi,f) = \sum_{m=0}^{M-1}\left[\left\{ w_{\mathrm{R},m}^{*}\frac{1+\cos\theta}{2}\exp(j\varphi) - w_{\mathrm{L},m}^{*}\frac{1-\cos\theta}{2}\exp(-j\varphi)\right\}\exp\left(-j\frac{2\pi}{f_{\mathrm{s}}}mf\right)\right]. \tag{14}$$

Because K and G_0 are constants, $g_{\mathrm{R}}(\theta,\varphi,f)$ can be considered as the gain pattern with respect to the RHCP signal. In a similar manner, the gain patterns with respect to the LHCP and LP signals can be obtained as follows:

$$\begin{aligned} g_{\mathrm{L}}(\theta,\varphi,f) &= \sum_{m=0}^{M-1}\left[\left\{ -w_{\mathrm{R},m}^{*}\frac{1-\cos\theta}{2}\exp(j\varphi) + w_{\mathrm{L},m}^{*}\frac{1+\cos\theta}{2}\exp(-j\varphi)\right\}\exp\left(-j\frac{2\pi}{f_{\mathrm{s}}}mf\right)\right] \\ g_{\mathrm{Lin}}(\theta,\varphi,\alpha,f) &= \sum_{m=0}^{M-1}\left[\left\{ w_{\mathrm{R},m}^{*}\frac{\cos\theta\cos\alpha + j\sin\alpha}{\sqrt{2}}\exp(j\varphi) + w_{\mathrm{L},m}^{*}\frac{\cos\theta\cos\alpha - j\sin\alpha}{\sqrt{2}}\exp(-j\varphi)\right\}\exp\left(-j\frac{2\pi}{f_{\mathrm{s}}}mf\right)\right] \end{aligned}. \tag{15}$$

The gain patterns corresponding to the three polarizations in (14) and (15) can be used for a performance demonstration. As the gains are three- or four-dimensional, more than one or two variables need to remain constant to generate two dimensional plots. If we fix φ of $g_{\mathrm{R}}(\theta,\varphi,f)$ or $g_{\mathrm{L}}(\theta,\varphi,f)$ to that of the RHCP or LHCP interference, or fix φ and α of $g_{\mathrm{Lin}}(\theta,\varphi,\alpha,f)$ to those of the LP interference, we can obtain the angle–frequency responses corresponding to the three polarizations. Likewise, when all variables of the gain patterns, except for f, are fixed, we can find the frequency responses. These two responses are provided as simulation results.

SIMULATION RESULTS

In order to demonstrate the interference mitigation capability of the proposed method, simulations were performed for an interference scenario in which one wideband and three narrowband interference sources are injected. The polarizations, directions, and frequencies of the interference sources are given in Table 1. In this scenario, the GPS signal incident from $(\theta = 40°, \varphi = 80°)$ was down-converted to 0.8 MHz, and the sampling frequency was set to 5 MHz. The number of FIR filter time taps was eight, and the interference-to-signal power ratio (ISR) of each jamming signal was set to 55 dB. The carrier-to-noise-density ratio (C/N_0) of the GPS signals was set to 45 dB-Hz, and the simulation was performed for 3 ms.

Table 1. Wideband and narrowband interference signals injected in the test scenario

Type	Polarization	Direction (θ,φ)	Intermediate frequency
Wideband	RHCP	$(\theta_{\mathrm{WB}} = 60°, \varphi_{\mathrm{WB}} = 10°)$	0.4 MHz
Narrowband	RHCP	$(\theta_{\mathrm{NB1}} = 70°, \varphi_{\mathrm{NB1}} = -40°)$	$f_{\mathrm{NB1}} = -1.4$ MHz
Narrowband	LHCP	$(\theta_{\mathrm{NB2}} = 60°, \varphi_{\mathrm{NB2}} = 120°)$	$f_{\mathrm{NB2}} = 1.3$ MHz
Narrowband	LP ($\alpha_{\mathrm{NB3}} = 45°$)	$(\theta_{\mathrm{NB3}} = 50°, \varphi_{\mathrm{NB3}} = -10°)$	$f_{\mathrm{NB3}} = 2.3$ MHz

The resulting angle–frequency response corresponding to the RHCP wideband interference for a fixed $\theta = \theta_{\mathrm{WB}}$, which is $g_{\mathrm{R}}(\theta_{\mathrm{WB}}, \varphi, f)$, is shown in Figure 4.

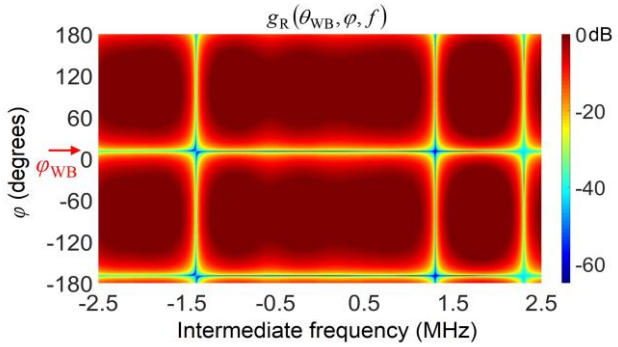

Figure 4: Angle–frequency response for the interference scenario. A spatial null is placed in the direction of the wideband interference, i.e., $\varphi = 10°$. Note that an additional unexpected null is also present at $\varphi = -170°$.

As can be seen in Figure 4, a spatial null (i.e., low gain throughout the frequency range) is placed in the wideband interference direction, that is, $\varphi = 10°$. The appearance of this spatial null shows that our single-element dual-polarized antenna method can mitigate one source of wideband interference. However, there is also an unexpected null in another direction, $\varphi = -170°$. This null pair occurs due to the symmetry of the RHCP gain pattern derived in (14). Because $g_{\mathrm{R}}(\theta, \varphi, f)$ is linearly dependent on $\cos\varphi$ and $\sin\varphi$ for a fixed θ, $g_{\mathrm{R}}(\theta, \varphi, f)$ has the following symmetry:

$$\left| g_{\mathrm{R}}(\theta, \varphi, f) \right| = \left| g_{\mathrm{R}}(\theta, \varphi \pm 180°, f) \right|. \tag{16}$$

Because both $g_{\mathrm{L}}(\theta, \varphi, f)$ and $g_{\mathrm{Lin}}(\theta, \varphi, \alpha, f)$ have a similar property to (16), the paired nulls can be also observed when LHCP or LP wideband interference impinges.

Due to this symmetry, a side effect can occur in a specific situation. If an RHCP wideband interference is incident with φ_0 and a GNSS signal impinges on the paired direction (i.e., $\varphi_0 \pm 180°$), the receiver fails to track the GNSS signal because of the paired null. Therefore, up to two GNSS satellites (one with the φ_0 direction and the other with the $\varphi_0 \pm 180°$ direction) can be lost. However, as the GNSS receiver has multiple tracking channels and each channel computes its own weight vector, other channels, which track other GNSS signals from different directions, are not affected. Moreover, the probability of two GNSS satellites having exactly the same and paired direction with respect to the interference direction simultaneously is very low; thus, the effect of the paired nulls on the receiver performance is not significant.

In addition, frequency notches generated at the frequencies of the narrowband interference are also observed, even though the second and third narrowband interference signals have different polarizations (i.e., LHCP and LP). Because the DOF obtained from the polarization diversity was consumed to generate a spatial null toward the wideband interference, the narrowband interference is suppressed only in the frequency domain, regardless of polarization. For this reason, three frequency notches are present in Figure 4.

The depths of the frequency notches can be observed in more detail at the frequency responses, which are $g_{\mathrm{R}}(\theta_{\mathrm{NB1}}, \varphi_{\mathrm{NB1}}, f)$, $g_{\mathrm{L}}(\theta_{\mathrm{NB2}}, \varphi_{\mathrm{NB2}}, f)$, and $g_{\mathrm{Lin}}(\theta_{\mathrm{NB3}}, \varphi_{\mathrm{NB3}}, \alpha_{\mathrm{NB3}}, f)$, as depicted in Figure 5.

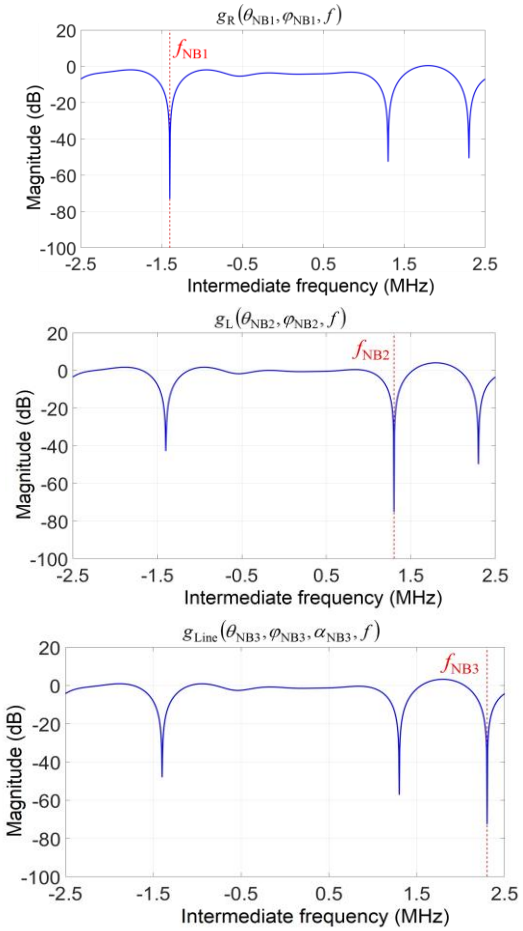

Figure 5: Frequency responses corresponding to the polarizations and directions of the three narrowband interference signals (top: RHCP narrowband interference; middle: LHCP narrowband interference; bottom: LP narrowband interference). Notches greater than 60 dB are generated at the intermediate frequencies of the respective narrowband interference signals.

As shown in Figure 5, the deepest notches are generated at the frequencies of all three narrowband interference signals, and the depth of the deepest notch in each frequency response is deeper than 60 dB. Because the ISR is 55 dB, the notches generated by the proposed method are deep enough to mitigate the narrowband interference, and these results prove that our method is able to 1) mitigate both wideband and narrowband interference simultaneously and 2) deal with interference of three polarizations (RHCP, LHCP, and LP) simultaneously.

In Figure 6, the signal to interference-plus-noise power ratio (SINR) is illustrated, and each SINR value is computed every 0.1 ms.

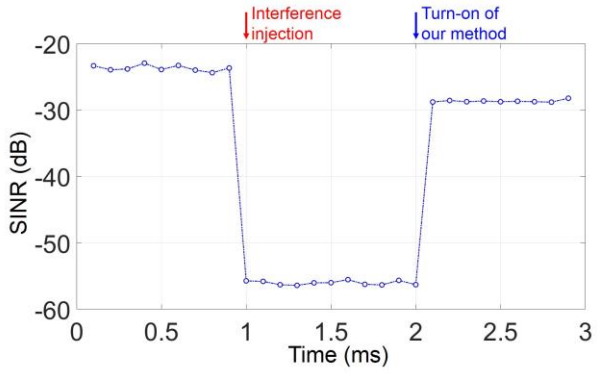

Figure 6: SINR vs. time. The interference signals are injected at 1 ms, and the proposed method is applied at 2 ms.

As shown in Figure 6, even though the SINR decreased by about 35 dB when the four interference signals are injected at 1 ms, the SINR was recovered by about 30 dB after the proposed method is applied. This SINR result quantitatively demonstrates the interference mitigation performance of our method.

CONCLUSION

In this paper, we presented an adaptive signal processing method based on a single-element dual-polarized antenna. The proposed algorithm is capable of mitigating one wideband interference source by generating a spatial null based on the polarization diversity of the dual-polarized antenna, and is also able to suppress multiple narrowband interference signals by placing frequency notches. The polarizations of the multiple interference sources, which can be mitigated by our method simultaneously, can be any combination of RHCP, LHCP, and LP. We derived mathematical models of the received RHCP, LHCP, and LP signals by taking the radiation pattern and polarization of the receiving antenna into consideration, and also described an LMS-based signal processing method, which has a similar functionality to STAP. The optimal weight vector was obtained without any previous knowledge of either interference direction or polarization, and a single weight vector can generate both a spatial null toward the wideband interference and multiple frequency notches at the frequencies of the narrowband interference signals simultaneously. The angle–frequency response, frequency response, and SINR plots were provided as simulation results, and these results demonstrated the interference mitigation performance of the proposed method. It was also shown that it is possible for up to two GNSS satellites to be lost in a specific situation, though its impact is not significant.

ACKNOWLEDGMENTS

This work has been supported by the National GNSS Research Center program of the Defense Acquisition Program Administration and Agency for Defense Development. This research was also supported by the Ministry of Science, ICT, and Future Planning (MSIP), Korea, under the "IT Consilience Creative Program" (IITP-2017-2017-0-01015), supervised by the Institute for Information & Communications Technology Promotion (IITP).

REFERENCES

[1] A. Grant, P. Williams, N. Ward, S. Basker, "GPS jamming and the impact on maritime navigation," *Journal of Navigation*, vol. 62, no. 2, pp. 173–187, 2009.

[2] D. S. De Lorenzo, S. C. Lo, J. Seo, Y.-H. Chen, P. K. Enge, "The WAAS/L5 signal for robust time transfer: Adaptive beamsteering antennas for satellite time synchronization," In Proceedings of the ION GNSS, Portland, OR, USA, September 2010, pp. 2106–2116.

[3] Y.-H. Chen, J.-C. Juang, D. S. De Lorenzo, J. Seo, S. Lo, P. Enge, D. M. Akos, "Real-time software receiver for GPS controlled reception pattern antenna array processing," In Proceedings of the ION GNSS, Portland, OR, USA, September 2010, pp. 1932–1941.

[4] Y.-H. Chen, J.-C. Juang, D. S. De Lorenzo, J. Seo, S. Lo, P. Enge, D. M. Akos, "Real-time dual-frequency (L1/L5) GPS/WAAS software receiver," In Proceedings of the ION GNSS, Portland, OR, USA, September 2011, pp. 767–774.

[5] P.-W. Son, J. H. Rhee, J. Seo, "Novel multi-chain-based Loran positioning algorithm for resilient navigation," *IEEE Transactions on Aerospace and Electronic Systems*, in press.

[6] D. Yoon, C. Kee, J. Seo, B. Park, "Position accuracy improvement by implementing the DGNSS-CP algorithm in smartphones," *Sensors*, vol. 16, no. 6, art. no. 910, 2016.

[7] M. S. Braash, A. J. van Dierendonck, "GPS receiver architectures and measurements," *Proceedings of the IEEE*, vol. 87, no. 1, pp. 48–64, 1999.

[8] J. Lee, Y. T. Morton, J. Lee, H.-S. Moon, J. Seo, "Monitoring and mitigation of ionospheric anomalies for GNSS-based safety critical systems," *IEEE Signal Processing Magazine*, vol. 34, no. 5, pp. 96-110, 2017.

[9] J. Seo, T. Walter, "Future dual-frequency GPS navigation system for intelligent air transportation under strong ionospheric scintillation," *IEEE Transactions on Intelligent Transportation Systems*, vol. 15, no. 5, pp. 2224-2236, 2014.

[10] Y. Jiao, D. Xu, Y. Morton, C. Rino, "Equatorial scintillation amplitude fading characteristics across the GPS frequency bands," *Navigation, Journal of the Institute of Navigation*, vol. 63, no. 3, pp. 267-281, 2016.

[11] J. Seo, T. Walter, P. Enge, "Availability impact on GPS aviation due to strong ionospheric scintillation," *IEEE Transactions on Aerospace and Electronic Systems*, vol. 47, no. 3, pp. 1963-1973, 2011.

[12] T.-Y. Chiou, J. Seo, T. Walter, P. Enge, "Performance of a Doppler-aided GPS navigation system for aviation applications under ionospheric scintillation," In Proceedings of the ION GNSS, Savannah, GA, USA, September 2008, pp. 490–498.

[13] J. Seo, J. Lee, S. Pullen, P. Enge, S. Close, "Targeted parameter inflation within ground-based augmentation systems to minimize anomalous ionospheric impact," *Journal of Aircraft*, vol. 49, no. 2, pp. 587-599, 2012.
[14] H. Xu, X. Cui, J. Shen, M. Lu, "A two-step beam-forming method based on carrier phases for GNSS adaptive array anti-jamming," In Proceedings of the ION ITM, Monterey, CA, USA, January 2016, pp. 793–804.
[15] O. C. Dabak, F. Erdem, T. Sonmez, L. Alatan, S. S. Koc, "Interference suppression in a GPS receiver with 4 element array design and implementation of beamforming algorithms," In Proceedings of the IEEE/ION PLANS, Savannah, GA, USA, April 2016, pp. 645–652.
[16] T. Lück, G. Heinrichs, A. Hornbostel, "Adaptively steered antenna array and receiver testing with multi-RF output GNSS simulator NavX® -NCS professional," In Proceedings of the ION GNSS, Tampa, FL, USA, September 2014, pp. 363–371.
[17] Q. Han, J. Pang, J. Nie, F. Wang, "Influence of interference type upon adaptive GNSS antenna array performance," In Proceedings of the IEEE/ION PLANS, Monterey, CA, USA, May 2014, pp. 1057–1064.
[18] G. X. Gao, L. Heng, A. Hornbostel, H. Denks, M. Meurer, T. Walter, P. Enge, "DME/TACAN interference mitigation for GNSS: algorithms and flight test results," *GPS Solutions*, vol. 17, no. 4, pp. 561–573, 2013.
[19] C. L. Chang. "Modified compressive sensing approach for GNSS signal reception in the presence of interference," *GPS Solutions*, vol. 20, no. 2, pp. 201–213, 2016.
[20] R. Rifkin, J. J. Vaccaro, "Comparison of narrowband adaptive filter technologies for GPS," In Proceedings of the IEEE PLANS, San Diego, CA, USA, March 2000, pp. 125–131.
[21] M. R. Mosavi, F. Shafiee, "Narrowband interference suppression for GPS navigation using neural networks," *GPS Solutions*, vol. 20, no. 3, pp. 341–351, 2016.
[22] J. Seo, Y.-H. Chen, D. S. De Lorenzo, S. Lo, P. Enge, D. Akos, J. Lee, "A real-time capable software-defined receiver using GPU for adaptive anti-jam GPS sensors," *Sensors*, vol. 11, no. 9, pp. 8966–8991, 2011.
[23] Y.-H. Chen, J.-C. Juang, J. Seo, S. Lo, D. M. Akos, D. S. De Lorenzo, P. Enge, "Design and implementation of real-time software radio for anti-interference GPS/WAAS sensors," *Sensors*, vol. 12, no. 10, pp. 13417–13440, 2012.
[24] M. W. Rosen, M. S. Braasch, "Low-cost GPS interference mitigation using single aperture cancellation techniques," In Proceedings of the ION NTM, Long Beach, CA, USA, January 1998, pp. 47–58.
[25] T. Kraus, F. Ribbehege, B. Eissfeller, "Use of the signal polarization for anti-jamming and anti-spoofing with a single antenna," In Proceedings of the ION GNSS, Tampa, FL, USA, September 2014, pp. 3495–3501.
[26] E. McMilin, Y.-H. Chen, D. S. De Lorenzo, S. Lo, D. Akos, P. Enge, "Field test validation of single-element antenna with anti-jam and spoof detection," In Proceedings of the ION GNSS, Tampa, Florida, September 2015, pp. 3314–3324.
[27] S. Haykin, "Adaptive Filter Theory," 4th ed., Prentice Hall, 2004.
[28] C. A. Balanis, "Antenna Theory: Analysis and Design," 3rd ed., Wiley, 2005.
[29] W. L. Stutzman, "Polarization in Electromagnetic Systems, Artech House, 1992.
[30] D. S. Cox, "Antenna diversity performance in mitigating the effects of portable radiotelephone orientation and multipath propagation," *IEEE Transactions on Communications*, vol. 31, no. 5, pp. 620–628, 1983.
[31] R. Goossens, H. Rogier, "Direction-of-arrival and polarization estimation with uniform circular arrays in the presence of mutual coupling," *AEU - International Journal of Electronics and Communications*, vol. 62, no. 3, pp. 199–206, 2008.